Available online at www.sciencedirect.com

SCIENCE DIRECT®

Journal of Computational Physics 201 (2004) 630–650

JOURNAL OF COMPUTATIONAL PHYSICS

www.elsevier.com/locate/jcp

Dirichlet-to-Neumann boundary conditions for multiple scattering problems ☆

Marcus J. Grote *, Christoph Kirsch

Department of Mathematics, University of Basel, Rheinsprung 21, CH-4051 Basel, Switzerland

Received 17 March 2004; received in revised form 21 June 2004; accepted 21 June 2004
Available online 13 August 2004

Abstract

A Dirichlet-to-Neumann (DtN) condition is derived for the numerical solution of time-harmonic multiple scattering problems, where the scatterer consists of several disjoint components. It is obtained by combining contributions from multiple purely outgoing wave fields. The DtN condition yields an exact non-reflecting boundary condition for the situation, where the computational domain and its exterior artificial boundary consist of several disjoint components. Because each sub-scatterer can be enclosed by a separate artificial boundary, the computational effort is greatly reduced and becomes independent of the relative distances between the different sub-domains. The DtN condition naturally fits into a variational formulation of the boundary-value problem for use with the finite element method. Moreover, it immediately yields as a by-product an exact formula for the far-field pattern of the scattered field. Numerical examples show that the DtN condition for multiple scattering is as accurate as the well-known DtN condition for single scattering problems [J. Comput. Phys. 82 (1989) 172; Numerical Methods for Problems in Infinite Domains, Elsevier, Amsterdam, 1992], while being more efficient due to the reduced size of the computational domain.

MSC: 65N99; 74J20; 78A45
Keywords: Time-harmonic scattering; Helmholtz equation; Unbounded domain; Non-reflecting boundary condition; Multiple scattering

☆ This work is partially supported by the Swiss National Science Foundation.
* Corresponding author.
E-mail addresses: Marcus.Grote@unibas.ch (M.J. Grote), Christoph.Kirsch@unibas.ch (C. Kirsch).

0021-9991/$ - see front matter
doi:10.1016/j.jcp.2004.06.012

1. Introduction

For the numerical solution of scattering problems in infinite domains, a well-known approach is to enclose all obstacles, inhomogeneities and nonlinearities with an artificial boundary B. A boundary condition is then imposed on B, which leads to a numerically solvable boundary-value problem in a finite domain Ω. The boundary condition should be chosen such that the solution of the problem in Ω coincides with the restriction to Ω of the solution in the original unbounded region.

If the scatterer consists of several obstacles, which are well separated from each other, the use of a single artificial boundary to enclose the entire scattering region, becomes too expensive. Instead it is preferable to enclose every sub-scatterer by a separate artificial boundary B_j. Then we seek an exact boundary condition on $B = \cup B_j$, where each B_j surrounds a single computational sub-domain Ω_j. This boundary condition must not only let outgoing waves leave Ω_j without spurious reflection from B_j, but also propagate the outgoing wave from Ω_j to all other sub-domains Ω_ℓ, which it may reenter subsequently. To derive such an exact boundary condition, an analytic expression for the solution everywhere in the exterior region is needed. Neither absorbing boundary conditions [1,2], nor perfectly matched layers [3–5] provide us with such a representation. Instead we shall seek a Dirichlet-to-Neumann (DtN) boundary condition, which is based on a Fourier series representation of the solution in the exterior region.

Exact DtN conditions have been derived for various equations and geometries, but always in the situation of a single computational domain, where the scattered field is purely outgoing outside Ω [6–10]. In a situation of multiple disjoint computational domains, however, waves are not purely outgoing outside the computational domain $\Omega = \cup\Omega_j$, as they may bounce back and forth between domains. We shall show how to overcome this difficulty and derive an exact DtN condition for multiple scattering. The derivation presented below for the Helmholtz equation in two space dimensions readily extends to multiple scattering problems in other geometries and also to different equations. Because this exact boundary condition allows the size of the computational sub-domains, Ω_j, to be chosen independently of the relative distances between them, the computational domain, Ω, can be chosen much smaller than that resulting from the use of a single, large computational domain.

There is an extended literature on the solution of multiple scattering problems – see Martin [11] for an introduction and overview. Due to the difficulties mentioned above, numerical methods used for multiple scattering so far have mainly been based on integral representations [12,13], while in the single scattering case many alternative methods, such as absorbing boundary conditions, perfectly matched layers, or the DtN approach are known. To our knowledge, this work constitutes the first attempt to generalize the well-known DtN approach to multiple scattering.

Some of the analytical techniques we shall use, have been known in the "classical" scattering literature for quite some time. For instance, in 1913 Záviška [14] considered multiple scattering from an array of parallel circular cylinders. He derived an infinite linear system for the unknown Fourier coefficients of the scattered field, which involve Fourier expansions of the purely outgoing wave fields about individual cylindrical obstacles. This method can be generalized to cylinders with non-circular cross-sections [15]. Another class of methods is based on single and double layer potentials, which involve integration with the Green's function over the artificial boundary. From this representation, systems of integral equations can be derived for multiple scattering problems – see Twersky [16] and Burke and Twersky [17] for an extensive overview of previous work until 1964, and [11] for more recent references.

In Section 2, we derive the DtN and modified DtN map for two scatterers. We show that the solution to the boundary value problem in Ω, with the DtN condition imposed on B, coincides with the restriction to Ω of the solution in the unbounded region Ω_∞. The formulation is generalized to an arbitrary number of scatterers in Section 3. In Section 4, we state a variational formulation of the artificial boundary-value problem for use with the finite element method. An explicit formula for the far-field pattern of the solution, based on the decomposition of the scattered field into multiple purely outgoing wave fields, is derived in Section 5. Finally, in Section 6, we consider a finite difference implementation of the multiple-DtN method and demonstrate its accuracy and convergence. We also compare the multiple-DtN approach to the well-known (single-)DtN method and show that both the numerical solutions and the far-field patterns, obtained by these two different methods, coincide.

2. Two scatterers

We consider acoustic wave scattering from two bounded disjoint scatterers in unbounded two-dimensional space. Each scatterer may contain one or several obstacles, inhomogeneities, and nonlinearity. We let Γ denote the piecewise smooth boundary of all obstacles and impose on Γ a Dirichlet-type boundary condition, for simplicity. In Ω_∞, the region outside Γ, the scattered field $u = u(r,\theta)$ then solves the exterior boundary-value problem

$$\Delta u + k^2 u = f \quad \text{in } \Omega_\infty \subset \mathbb{R}^2, \tag{1}$$

$$u = g \quad \text{on } \Gamma, \tag{2}$$

$$\lim_{r\to\infty} \sqrt{r}\left(\frac{\partial}{\partial r} - \mathrm{i}k\right)u = 0. \tag{3}$$

The wave number k and the source term f may vary in space, while f may be nonlinear. The Sommerfeld radiation condition (3) ensures that the scattered field corresponds to a purely outgoing wave at infinity.

Next, we assume that both scatterers are *well separated*, that is we assume that we can surround them by two non-intersecting circles B_1, B_2 centered at c_1, c_2 with radii R_1, R_2, respectively. In the unbounded region D, outside the two circles, we assume that the wave number $k > 0$ is constant and that f vanishes. In D, the scattered field u thus satisfies

$$\Delta u + k^2 u = 0 \quad \text{in } D, \quad k > 0 \text{ constant}, \tag{4}$$

$$\lim_{r\to\infty} \sqrt{r}\left(\frac{\partial}{\partial r} - \mathrm{i}k\right)u = 0. \tag{5}$$

We wish to compute the scattered field, u, in the computational domain $\Omega = \Omega_\infty \backslash D$, which consists of the two disjoint components Ω_1 and Ω_2. A typical configuration with two obstacles is shown in Fig. 1. Here, the computational domain Ω is internally bounded by $\Gamma = \Gamma_1 \cup \Gamma_2$, and externally by $B = \partial D$, which consists of the two circles B_1 and B_2.

To solve the scattering problem (1)–(3) inside Ω, a boundary condition is needed at the exterior artificial boundary B. This boundary condition must ensure that the solution in Ω, with that boundary condition imposed on B, coincides with the restriction of the solution in the original unbounded region Ω_∞.

2.1. Derivation of the DtN map

On B we shall now derive a DtN map, which establishes an exact relation between the values of u and its normal derivative. In contrast to the case of a single circular artificial boundary, as considered for example by Givoli [7] and Grote and Keller [8], we cannot simply expand u outside B in a Fourier series. First, there is no separable coordinate system outside B for the Helmholtz equation [18] and second, u is not purely outgoing in D. Indeed, part of the scattered field leaving Ω_1 will reenter Ω_2, and vice versa. Hence the boundary condition we seek on B must not only let outgoing waves leave Ω_1 without spurious reflection

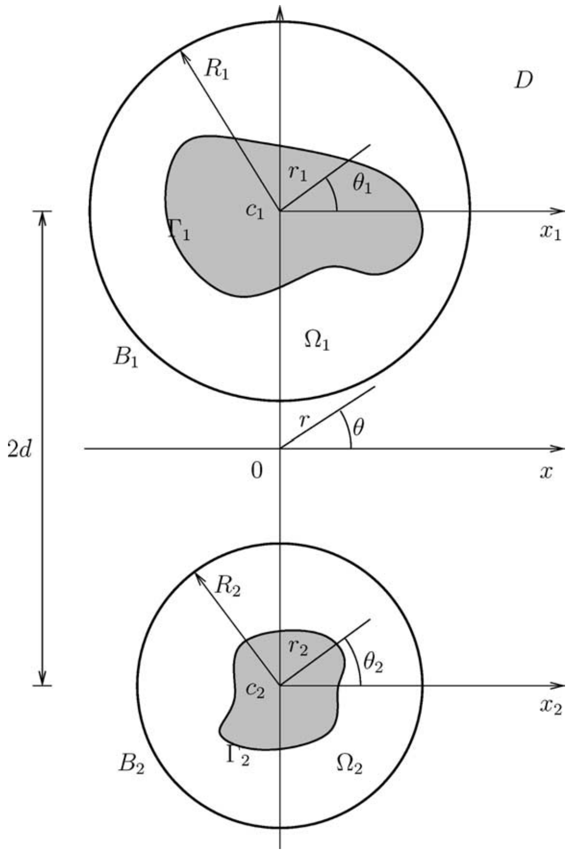

Fig. 1. A typical configuration with two obstacles bounded by Γ_1 and Γ_2 is shown. The computational domain $\Omega = \Omega_1 \cup \Omega_2$ is externally bounded by the artificial boundary $B = B_1 \cup B_2$. In each domain component Ω_j, we use a local polar coordinate system (r_j,θ_j), while (r,θ) denotes the global polar coordinate system centered at the origin.

from B_1, but also propagate the outgoing wave field from Ω_1 to Ω_2, and vice versa, without any spurious reflection.

We begin the derivation of an exact non-reflecting boundary condition on $B = B_1 \cup B_2$ by introducing a local polar coordinate system (r_j, θ_j) outside each circle B_j, centered at c_j (see Fig. 1). Next, we denote by D_1 the unbounded domain outside B_1 with $r_1 > R_1$, and by D_2 the unbounded domain outside B_2 with $r_2 > R_2$. We now decompose the scattered field u in D into two purely outgoing wave fields u_1 and u_2, which solve the following problems:

$$\Delta u_1 + k^2 u_1 = 0 \quad \text{in } D_1, \tag{6}$$

$$\lim_{r\to\infty} \sqrt{r}\left(\frac{\partial}{\partial r} - \mathrm{i}k\right) u_1 = 0 \tag{7}$$

and

$$\Delta u_2 + k^2 u_2 = 0 \quad \text{in } D_2, \tag{8}$$

$$\lim_{r\to\infty} \sqrt{r}\left(\frac{\partial}{\partial r} - \mathrm{i}k\right) u_2 = 0. \tag{9}$$

Each wave field is influenced only by a single scatterer and completely obvious to the other. Therefore, u_1 and u_2 are entirely determined by their values on B_1 or B_2, respectively; they are given in local polar coordinates (r_1, θ_1), (r_2, θ_2) by

$$u_j(r_j, \theta_j) = \frac{1}{\pi} \sum_{n=0}^{\infty}{}' \frac{H_n^{(1)}(kr_j)}{H_n^{(1)}(kR_j)} \int_0^{2\pi} u_j(R_j, \theta') \cos n(\theta_j - \theta')\, \mathrm{d}\theta', \quad r_j \geqslant R_j, \tag{10}$$

for $j = 1, 2$. Here, the prime after the sum indicates that the term for $n = 0$ is multiplied by 1/2, while $H_n^{(1)}$ denotes the nth order Hankel function of the first kind. We now couple u_1 and u_2 with u by matching $u_1 + u_2$ with u on $B = B_1 \cup B_2$:

$$u_1 + u_2 = u \quad \text{on } B. \tag{11}$$

Both u and $u_1 + u_2$ solve the homogeneous Helmholtz equation (4) in $D = D_1 \cap D_2$, together with the Sommerfeld radiation condition (5) at infinity. Since u and $u_1 + u_2$ coincide on B, they coincide everywhere in the exterior region D. We summarize this result in the following proposition. Moreover, before proceeding with the derivation of the DtN map, we shall also prove that such a decomposition always exists and is unique.

Proposition 1. *Let u be the unique solution to the exterior Dirichlet problem (1)–(3) and assume that u satisfies* (4) *and* (5) *in the exterior region, D. Then*

$$u \equiv u_1 + u_2 \quad \text{in } B \cup D, \tag{12}$$

where u_1 and u_2 are solutions to the problems (6)–(9), respectively, together with the matching condition (11). The decomposition of u into the two purely outgoing wave fields u_1 and u_2 is unique.

Proof. By the argument above, we have already shown that if $u = u_1 + u_2$ on B, and u_1 and u_2 solve (6)–(9), then $u \equiv u_1 + u_2$ everywhere in D. We shall now show that u_1 and u_2 exist and, in fact, are unique.

Existence. In the exterior domain D, we use the Kirchhoff–Helmholtz formula [19] to write

$$u(x) = \int_B \left\{ u(y) \frac{\partial \Phi(x, y)}{\partial n(y)} - \frac{\partial u}{\partial n}(y) \Phi(x, y) \right\} \mathrm{d}s(y), \quad x \in D. \tag{13}$$

Here, Φ is the fundamental solution of the Helmholtz equation in two space dimensions,

$$\Phi(x, y) = \frac{\mathrm{i}}{4} H_0^{(1)}(k|x - y|), \quad x \neq y, \tag{14}$$

while n denotes the outward normal from Ω on the artificial boundary B. Let

$$u_j(x) := \int_{B_j} \left\{ u(y) \frac{\partial \Phi(x, y)}{\partial n(y)} - \frac{\partial u}{\partial n}(y) \Phi(x, y) \right\} \mathrm{d}s(y), \quad x \in D_j, \tag{15}$$

for $j = 1, 2$. Then, a straightforward calculation shows that u_1 satisfies (6) and (7) whereas u_2 satisfies (8) and (9). Clearly, $u(x) = u_1(x) + u_2(x)$, $\forall x \in D = D_1 \cap D_2$. The expressions (13) and (15) can be continuously extended up to the artificial boundaries B and B_1, B_2, respectively [20, Theorem 2.13]. Thus, u_1 and u_2 also satisfy the matching condition (11).

Uniqueness. Following a suggestion of S. Tordeux (INRIA, private communication, July 2003), we let $u \equiv v_1 + v_2$ be another decomposition in $B \cup D$, where v_1 and v_2 solve (6)–(9), respectively. We shall now show that $v_1 \equiv u_1$ and that $v_2 \equiv u_2$ throughout D. To do so, we let $w_1 := u_1 - v_1$ and $w_2 := u_2 - v_2$. Hence, w_1 and w_2 satisfy (6)–(9), respectively. Because w_2 is regular throughout D_2, it is also regular, and therefore bounded, everywhere inside B_1, including the local origin, c_1. Thus, in the vicinity of B_1, w_1 and w_2 can be written in the local polar coordinates, (r_1, θ_1), as

$$w_1(r_1,\theta_1) = \sum_{n\in\mathbb{Z}} a_n H_n^{(1)}(kr_1)\,\mathrm{e}^{\mathrm{i}n\theta_1}, \tag{16}$$

$$w_2(r_1,\theta_1) = \sum_{n\in\mathbb{Z}} b_n J_n(kr_1)\,\mathrm{e}^{\mathrm{i}n\theta_1} \tag{17}$$

for $r_1 \in I := [R_1, R_1 + \varepsilon]$, with $\varepsilon = |c_2 - c_1| - (R_1 + R_2) > 0$, because the scatterers are assumed to be well separated. From the uniqueness of u we obtain $w_1 + w_2 = u_1 + u_2 - (v_1 + v_2) \equiv 0$ in $B \cup D$. Therefore

$$a_n H_n^{(1)}(kr_1) + b_n J_n(kr_1) = 0 \quad \forall n \in \mathbb{Z},\ \ r_1 \in I. \tag{18}$$

Since $H_n^{(1)}$ and J_n are two linearly independent solutions of Bessel's differential equation, we conclude that $a_n = b_n = 0$ for all $n \in \mathbb{Z}$. Thus, $v_1 \equiv u_1$ and $v_2 \equiv u_2$ in $B \cup D$. □

As a consequence of the proposition, we can now explicitly determine a DtN map for u by differentiating u with respect to the outward normal n on B_1 and B_2 as follows:

$$\partial_n u = M[u_1] + T[u_2] \quad \text{on } B_1, \tag{19}$$

$$\partial_n u = M[u_2] + T[u_1] \quad \text{on } B_2, \tag{20}$$

$$u_1 + P[u_2] = u \quad \text{on } B_1, \tag{21}$$

$$P[u_1] + u_2 = u \quad \text{on } B_2. \tag{22}$$

Here the operator M corresponds to the *standard single-DtN operator*

$$M[u_j](\theta_j) := \frac{1}{\pi}\sum_{n=0}^{\infty\prime} \frac{kH_n^{(1)'}(kR_j)}{H_n^{(1)}(kR_j)} \int_0^{2\pi} u_j(R_j,\theta')\cos n(\theta_j - \theta')\,\mathrm{d}\theta', \tag{23}$$

$j = 1, 2$. The *transfer operator* T and *propagation operator* P are given by

$$T[u_1](\theta_2) := \frac{\partial u_1}{\partial r_2}(R_2,\theta_2), \quad T[u_2](\theta_1) := \frac{\partial u_2}{\partial r_1}(R_1,\theta_1), \tag{24}$$

$$P[u_1](\theta_2) := u_1(R_2,\theta_2), \quad P[u_2](\theta_1) := u_2(R_1,\theta_1). \tag{25}$$

The expressions on the right-hand sides of (19), (20) and on the left-hand sides of (21), (22) can be evaluated explicitly by using the definitions (23)–(25) and the (exact) Fourier representation (10), valid in each local coordinate system. These calculations involve some technical but straightforward coordinate transformations. For instance, in the particular situation shown in Fig. 1, $T[u_2]$ and $P[u_2]$ are explicitly given (in local polar (r_1,θ_1)-coordinates) on B_1 for $\theta_1 \in [0, 2\pi)$ by

$$\begin{aligned} T[u_2](\theta_1) = \frac{1}{r_2}\Bigg[&(R_1 + 2d\sin\theta_1)\frac{1}{\pi}\sum_{n=0}^{\infty\prime}\frac{kH_n^{(1)'}(kr_2)}{H_n^{(1)}(kR_2)}\int_0^{2\pi} u_2(R_2,\theta')\cos n(\theta_2-\theta')\,\mathrm{d}\theta' \\ &+ \frac{1}{r_2}2d\cos\theta_1\frac{1}{\pi}\sum_{n=0}^{\infty\prime}\frac{nH_n^{(1)}(kr_2)}{H_n^{(1)}(kR_2)}\int_0^{2\pi} u_2(R_2,\theta')\sin n(\theta_2-\theta')\,\mathrm{d}\theta'\Bigg], \end{aligned} \tag{26}$$

$$P[u_2](\theta_1) = \frac{1}{\pi}\sum_{n=0}^{\infty\prime}\frac{H_n^{(1)}(kr_2)}{H_n^{(1)}(kR_2)}\int_0^{2\pi} u_2(R_2,\theta')\cos n(\theta_2-\theta')\,\mathrm{d}\theta', \tag{27}$$

where

$$r_2 = \sqrt{R_1^2 + 4dR_1 \sin\theta_1 + 4d^2}, \tag{28}$$

$$\sin\theta_2 = \frac{1}{r_2}(R_1 \sin\theta_1 + 2d), \tag{29}$$

$$\cos\theta_2 = \frac{1}{r_2} R_1 \cos\theta_1. \tag{30}$$

The expressions for $T[u_1]$ and $P[u_1]$ on B_2 are similar to (26)–(30), with r_2 replaced by r_1, θ_2 by θ_1, etc.

The matching condition (21), (22) cannot be inverted explicitly, and u_1 and u_2 thereby eliminated from the DtN condition (19)–(22). Instead, we shall compute the values of u_1 on B_1 and u_2 on B_2, in addition to the values of u. These auxiliary values are also useful during post-processing, as they yield explicit expressions both for u everywhere outside Ω and for its far-field pattern – see Section 5.

With the DtN condition given by (19)–(22), we now state the boundary value problem for u inside the computational domain $\Omega = \Omega_1 \cup \Omega_2$:

$$\Delta u + k^2 u = f \quad \text{in } \Omega, \tag{31}$$

$$u = g \quad \text{on } \Gamma, \tag{32}$$

$$\partial_n u = M[u_1] + T[u_2] \quad \text{on } B_1, \tag{33}$$

$$\partial_n u = M[u_2] + T[u_1] \quad \text{on } B_2, \tag{34}$$

$$u_1 + P[u_2] = u \quad \text{on } B_1, \tag{35}$$

$$P[u_1] + u_2 = u \quad \text{on } B_2. \tag{36}$$

We now show that this boundary value problem has a unique solution, which coincides with the solution to the original problem (1)–(3).

Theorem 2. *Let u be the unique solution to the exterior Dirichlet problem (1)–(3) and assume that u satisfies* (4), (5) *in the exterior region, D. Then the two scatterer boundary value problem (31)–(36) has a unique solution in Ω, which coincides with the restriction of u to Ω.*

Proof. *Existence*. We shall show that $u|_\Omega$ is a solution to (31)–(36). Since u satisfies (1), (2) it trivially satisfies (31), (32). To show that $u|_\Omega$ satisfies the DtN condition (33)–(36) on B, we consider in $B \cup D$ the unique decomposition $u \equiv u_1 + u_2$, provided by Proposition 1. Since $u_1 + u_2$ satisfies the DtN boundary condition (33)–(36) on B, by construction, so does the restriction of u to Ω. Therefore, $u|_\Omega$ is a solution to the boundary value problem (31)–(36).

Uniqueness: We extend the argument of Harari and Hughes [21] for a single scatterer to the case of two scatterers. Let v, together with $v_1|_{B_1}$ and $v_2|_{B_2}$, denote another solution of (31)–(36). We shall show that $v \equiv u|_\Omega$. First, we denote by

$$\overline{v_j}(r_j, \theta_j) := \frac{1}{\pi} \sum_{n=0}^{\infty\prime} \frac{H_n^{(1)}(kr_j)}{H_n^{(1)}(kR_j)} \int_0^{2\pi} v_j(R_j, \theta') \cos n(\theta_j - \theta') \, \mathrm{d}\theta', \tag{37}$$

the two purely outgoing wave fields, defined for $r_j \geqslant R_j$, $j = 1,2$. Next, we construct an extension

$$\overline{v} := \begin{cases} v & \text{in } \Omega, \\ \overline{v_1} + \overline{v_2} & \text{in } B \cup D \end{cases} \tag{38}$$

of v into the exterior region D. We shall now show that $w := u - \overline{v}$ vanishes in Ω. To begin, we remark that w and its normal derivative are continuous everywhere in Ω_∞, while w satisfies $\Delta w + k^2 w = 0$ in Ω and $w = 0$ on Γ. By using integration by parts we now find that

$$\int_\Omega |\nabla w|^2 - k^2|w|^2 \, \mathrm{d}x = \int_B w \frac{\partial \overline{w}}{\partial n} \, \mathrm{d}s, \tag{39}$$

from which we infer that

$$\int_B w \frac{\partial \overline{w}}{\partial n} - \overline{w} \frac{\partial w}{\partial n} \, \mathrm{d}s = 0. \tag{40}$$

Let B_r denote the sphere of radius $r > 0$ centered at the origin. Again we use integration by parts, (40) and the fact that w is a solution of (4) to obtain

$$\begin{aligned} 0 &= \int_B w \frac{\partial \overline{w}}{\partial n} - \overline{w} \frac{\partial w}{\partial n} \, \mathrm{d}s = \int_D w \Delta \overline{w} - \overline{w} \Delta w \, \mathrm{d}x - \lim_{r\to\infty} \int_{B_r} w \frac{\partial \overline{w}}{\partial r} - \overline{w} \frac{\partial w}{\partial r} \, \mathrm{d}s \\ &= - \lim_{r\to\infty} \int_{B_r} w \frac{\partial \overline{w}}{\partial r} - \overline{w} \frac{\partial w}{\partial r} \, \mathrm{d}s. \end{aligned} \tag{41}$$

From the radiation condition (5) and (41), we now infer that

$$\begin{aligned} 0 &= \lim_{r\to\infty} \int_{B_r} \left| \sqrt{r} \left(\frac{\partial}{\partial r} - \mathrm{i}k \right) w \right|^2 \mathrm{d}s = \lim_{r\to\infty} r \int_{B_r} \left| \frac{\partial w}{\partial r} \right|^2 + k^2 |w|^2 - \mathrm{i}k \left(w \frac{\partial \overline{w}}{\partial r} - \overline{w} \frac{\partial w}{\partial r} \right) \mathrm{d}s \\ &= \lim_{r\to\infty} r \int_{B_r} \left| \frac{\partial w}{\partial r} \right|^2 + k^2 |w|^2 \, \mathrm{d}s. \end{aligned} \tag{42}$$

Since $k^2 > 0$ we conclude that

$$\lim_{r\to\infty} \int_{B_r} |w|^2 \, \mathrm{d}s = 0. \tag{43}$$

Eq. (43) then implies that $w \equiv 0$ in D, by Rellich's theorem [19, Lemma 2.11]. By continuity, we also have $w = 0$ on B. Finally, we apply Proposition 1 to w, which yields the unique decomposition $w \equiv w_1 + w_2$ with $w_1 \equiv 0$ and $w_2 \equiv 0$ in $B \cup D$. Because of the DtN condition (33)–(36) we conclude that $\partial_n w = 0$ on B. Since the problem

$$\Delta w + k^2 w = 0 \quad \text{in } \Omega, \tag{44}$$

$$w = 0 \quad \text{on } \Gamma, \tag{45}$$

$$w = 0 \quad \text{on } B, \tag{46}$$

$$\partial_n w = 0 \quad \text{on } B \tag{47}$$

has only the trivial solution (which is verified directly by expanding the solution of (44) in a Fourier series and by using the linear independence of the Hankel functions), $w \equiv 0$ in Ω or $v \equiv u|_\Omega$. □

2.2. The modified DtN map

In practice, the infinite sums which occur in the operators M, T, and P in the DtN condition (33)–(36) have to be truncated at some finite $N \geqslant 0$. The corresponding truncated operators are denoted by M^N, T^N, and P^N. Even in the situation of a single scatterer, truncation can destroy the uniqueness of the solution in

Ω with the truncated DtN condition imposed at B. For single scattering, Harari and Hughes showed that uniqueness is preserved if N is chosen large enough [21]. Alternatively, the modified DtN (MDtN) map introduced in [8] can be used to overcome this difficulty. Its generalization to the case of two scatterers is straightforward:

$$\partial_n u = \mathrm{i}ku + (M - \mathrm{i}k)^N[u_1] + (T - \mathrm{i}kP)^N[u_2] \quad \text{on } B_1, \tag{48}$$

$$\partial_n u = \mathrm{i}ku + (M - \mathrm{i}k)^N[u_2] + (T - \mathrm{i}kP)^N[u_1] \quad \text{on } B_2, \tag{49}$$

$$u_1 + P^N[u_2] = u \quad \text{on } B_1, \tag{50}$$

$$P^N[u_1] + u_2 = u \quad \text{on } B_2. \tag{51}$$

Numerical results with the MDtN map applied to multiple scattering are shown in Section 6.1. They corroborate the expected improvement in accuracy and stability, well-known in the single scatterer case.

3. Multiple scattering problems

The derivation of the DtN map presented above for two scatterers is easily generalized to the case of several scatterers. We consider a situation with J scatterers, and surround each scatterer by a circle B_j of radius R_j. Again we denote by $B = \bigcup_{j=1}^J B_j$ the entire artificial boundary and by D_j the unbounded region outside the jth circle. Hence the computational domain $\Omega = \bigcup_{j=1}^J \Omega_j$, where Ω_j denotes the finite computational region inside B_j, whereas $D = \bigcap_{j=1}^J D_j$ denotes the unbounded exterior region.

In D, we now split the scattered field into J purely outgoing wave fields $u_1, \ldots, u_J$, which solve the problems

$$\Delta u_j + k^2 u_j = 0 \quad \text{in } D_j, \tag{52}$$

$$\lim_{r\to\infty} \sqrt{r}\left(\frac{\partial}{\partial r} - \mathrm{i}k\right)u_j = 0 \tag{53}$$

for $j = 1, \ldots, J$. Thus u_j is entirely determined by its values on B_j; it is given in local polar coordinates (r_j, θ_j) by (10). The matching condition is now given by

$$\sum_{j=1}^{J} u_j = u \quad \text{on } B. \tag{54}$$

In analogy to Proposition 1, we can show that

$$u \equiv \sum_{j=1}^{J} u_j \quad \text{in } B \cup D \tag{55}$$

and that this decomposition is unique. Therefore, we immediately find the DtN map for a multiple scattering problem with J scatterers:

$$\partial_n u = M[u_j] + \sum_{\substack{\ell=1 \\ \ell\neq j}}^{J} T[u_\ell] \quad \text{on } B_j, \tag{56}$$

$$u_j + \sum_{\substack{\ell=1 \\ \ell \neq j}}^{J} P[u_\ell] = u \quad \text{on } B_j, \quad j = 1, \ldots, J. \tag{57}$$

Here M, T and P operate on the purely outgoing wave fields u_j as follows:

$$M : u_j|_{B_j} \mapsto \left.\frac{\partial u_j}{\partial r_j}\right|_{B_j}, \quad T : u_\ell|_{B_\ell} \mapsto \left.\frac{\partial u_\ell}{\partial r_j}\right|_{B_j}, \quad P : u_\ell|_{B_\ell} \mapsto u_\ell|_{B_j}. \tag{58}$$

We note that *no additional analytical derivations* due to coordinate transformations, etc. are needed once the situation of two scatterers has been resolved. Hence, the standard DtN operator M is given by (23), while the operators T and P are again given by (26)–(30), with '1' replaced by 'j' and '2' by 'ℓ', or vice versa.

In practice, the infinite series in the operators M, T and P need to be truncated at some finite value N_j, which can be different for each sub-domain Ω_j. We denote the corresponding truncated operators by M^{N_j}, T^{N_j} and P^{N_j}, $j = 1,\ldots,J$. For simplicity of notation, we shall assume that all boundary operators are truncated at the same value $N_j = N$, $j = 1,\ldots,J$.

We now extend the modified DtN map (48)–(51) to the situation of J scatterers:

$$\partial_n u = \mathrm{i}ku + (M - \mathrm{i}k)^N [u_j] + \sum_{\substack{\ell=1 \\ \ell \neq j}}^{J} (T - \mathrm{i}kP)^N [u_\ell] \quad \text{on } B_j, \tag{59}$$

$$u_j + \sum_{\substack{\ell=1 \\ \ell \neq j}}^{J} P^N [u_\ell] = u \quad \text{on } B_j, \tag{60}$$

where $N \geqslant 0$ is the truncation index.

For $J = 1$, the expressions in (56), (57) and (59), (60) reduce to the well-known DtN and modified DtN conditions for single scattering problems [6,8]. For $J = 2$, they correspond to the conditions derived previously in Section 2.

To further simplify the notation, we define the (symbolic) vectors

$$\partial_n u|_B = \left(\partial_{r_1} u|_{B_1}, \partial_{r_2} u|_{B_2}, \ldots, \partial_{r_J} u|_{B_J}\right)^{\mathrm{T}}, \tag{61}$$

$$u|_B = \left(u|_{B_1}, u|_{B_2}, \ldots, u|_{B_J}\right)^{\mathrm{T}}, \tag{62}$$

$$u_{\mathrm{out}}|_B = \left(u_1|_{B_1}, u_2|_{B_2}, \ldots, u_J|_{B_J}\right)^{\mathrm{T}} \tag{63}$$

and the operator matrices

$$\boldsymbol{T} = \left\{T_\ell^j\right\}_{j,\ell=1}^{J}, \quad T_\ell^j : u_\ell|_{B_\ell} \mapsto \partial_{r_j} u_\ell|_{B_j}, \tag{64}$$

$$\boldsymbol{P} = \left\{P_\ell^j\right\}_{j,\ell=1}^{J}, \quad P_\ell^j : u_\ell|_{B_\ell} \mapsto u_\ell|_{B_j} \tag{65}$$

With these notations we rewrite the DtN map (56), (57) in matrix-vector notation as

$$\partial_n u = \boldsymbol{T} u_{\mathrm{out}} \quad \text{on } B, \tag{66}$$

$$\boldsymbol{P} u_{\mathrm{out}} = u \quad \text{on } B, \tag{67}$$

and the modified DtN (MDtN) map (59), (60) as

$$\partial_n u = \mathrm{i}ku + (\boldsymbol{T} - \mathrm{i}k\boldsymbol{P})^N u_{\text{out}} \quad \text{on } B, \tag{68}$$

$$\boldsymbol{P}^N u_{\text{out}} = u \quad \text{on } B. \tag{69}$$

Remark. The derivation of the DtN (or MDtN) condition for multiple acoustic scattering can easily be generalized to different equations (Maxwell's equations [22], linear elasticity [10], etc), to other geometries (ellipsoidal [8], wave-guide [23]), or to three space dimensions. In fact, our approach can be extended to all multiple scattering problems, for which a DtN map is already known for single scattering.

4. Variational formulation

In the previous section, we have derived the DtN boundary condition (66), (67) for multiple scattering problems. We shall now show how to combine it with two different numerical schemes used in the interior. In this section, we present a variational formulation of a multiple scattering boundary value problem, which is needed for the numerical solution with any finite element scheme. In Section 6, we shall show how to combine the multiple-DtN boundary condition with a finite difference scheme. Numerical solutions obtained with the finite difference scheme are then compared with a finite element solution using the DtN method in a single larger domain.

We shall now show how to combine the multiple scattering DtN condition (66), (67) with the finite element method in Ω. The computational domain Ω is bounded in part by B, the union of J disjoint circles, and in part by some interior piecewise smooth boundary, Γ. For simplicity we consider a Dirichlet-type condition on Γ, and assume that the acoustic medium inside Ω is also homogeneous and isotropic. Hence the boundary value problem in Ω is:

$$-\Delta u - k^2 u = f \quad \text{in } \Omega, \tag{70}$$

$$u = g \quad \text{on } \Gamma, \tag{71}$$

$$\partial_n u = \boldsymbol{T} u_{\text{out}} \quad \text{on } B, \tag{72}$$

$$\boldsymbol{P} u_{\text{out}} = u \quad \text{on } B. \tag{73}$$

Next, we introduce the function spaces

$$V = \{v \in H^1(\Omega) | v|_\Gamma \equiv g\}, \tag{74}$$

$$V_0 = \{v \in H^1(\Omega) | v|_\Gamma \equiv 0\}. \tag{75}$$

To derive a variational formulation of (70)–(73) we multiply (70) by a test function $v \in V_0$ and integrate over Ω. Then we use integration by parts, together with (71)–(73), which yields the following variational formulation for (70)–(73):

Find $u \in V$ such that

$$(\nabla u, \nabla v)_\Omega - (k^2 u, v)_\Omega - (\boldsymbol{T} u_{\text{out}}, v)_B = (f, v)_\Omega, \tag{76}$$

$$(\boldsymbol{P} u_{\text{out}}, v)_B = (u, v)_B, \tag{77}$$

for all $v \in V_0$.

Here, $(\cdot,\cdot)_\Omega$ and $(\cdot,\cdot)_B$ denote the standard L^2-inner products on Ω and B, respectively.

For the finite element discretization of (76), (77) we choose a triangulation $\mathscr{T}_h$ of $\overline{\Omega}$, with mesh size $h > 0$ and nodes $\mathscr{N}(\mathscr{T}_h) = \mathscr{N}_\Omega \cup \mathscr{N}_\Gamma \cup \mathscr{N}_B$. Then we choose a subspace $V_N \subset V$ of finite dimension $N = |\mathscr{N}(\mathscr{T}_h)| = N_\Omega + N_\Gamma + N_B$, and nodal basis functions

$$\{\Phi_i\}_{i=1}^N \subset V_N, \quad \Phi_i(x_j) = \delta_{ij}, \quad x_j \in \mathscr{N}(\mathscr{T}_h). \tag{78}$$

We denote by u_Ω^h the values of the finite element solution on $\mathscr{N}_\Omega$, by u_B^h its values on $\mathscr{N}_B$ and by u_{out}^h the values of u_{out} – see (63) – on $\mathscr{N}_B$, which yields from (76), (77) the following linear system of equations:

$$\left(\begin{array}{c|c} \boldsymbol{K} & \begin{matrix}\mathbf{0}\\ -\boldsymbol{T}\end{matrix} \\ \hline \mathbf{0}\ -\boldsymbol{I} & \boldsymbol{P} \end{array}\right) \left(\begin{array}{c} u_\Omega^h \\ u_B^h \\ \hline u_{\mathrm{out}}^h \end{array}\right) = \left(\begin{array}{c} f \\ \hline 0 \end{array}\right) \tag{79}$$

Here $\boldsymbol{I}$ denotes the $N_B \times N_B$ identity matrix, while the other entries are given by

$$K_{ij} = (\nabla\Phi_j, \nabla\Phi_i)_\Omega - (k^2\Phi_j, \Phi_i)_\Omega, \quad i,j : x_i, x_j \in \mathscr{N}_\Omega \cup \mathscr{N}_B, \tag{80}$$

$$T_{ij} = (\boldsymbol{T}\Phi_j, \Phi_i)_B, \quad i,j : x_i, x_j \in \mathscr{N}_B, \tag{81}$$

$$P_{ij} = (\boldsymbol{P}\Phi_j, \Phi_i)_B, \quad i,j : x_i, x_j \in \mathscr{N}_B, \tag{82}$$

$$f_i = (f, \Phi_i)_\Omega - \sum_{j: x_j \in \mathscr{N}_\Gamma} g(x_j) K_{ij}, \quad i : x_i \in \mathscr{N}_\Omega \cup \mathscr{N}_B. \tag{83}$$

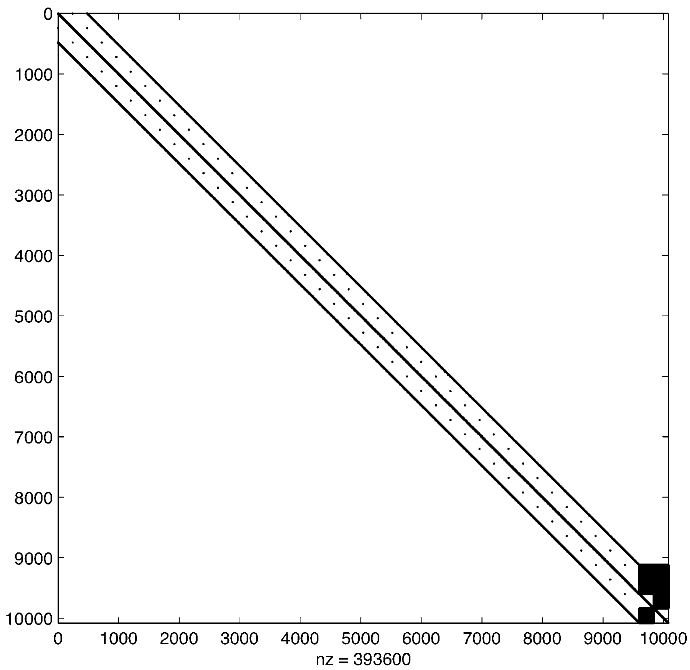

Fig. 2. The sparsity pattern of the finite difference matrix for a two scatterer problem. There are 21 layers of 240 grid points in each domain Ω_1 and Ω_2. Hence the total number of unknowns is $2 \times (21 \times 240)$ for u plus 2×240 for $u_1|_{B_1}$ and $u_2|_{B_2}$.

Because the nodal basis functions $\{\Phi_j\}_{j=1}^{N}$ are local, $\boldsymbol{K}$ is a sparse real $((N_\Omega + N_B) \times (N_\Omega + N_B))$-matrix. The $(N_B \times N_B)$-matrices $\boldsymbol{T}$ and $\boldsymbol{P}$, however, have complex valued entries and are full, because the DtN condition couples all unknowns on B. Clearly the structure of $\boldsymbol{K}$, $\boldsymbol{T}$, and $\boldsymbol{P}$ will depend both on the number of sub-scatterers and on the finite element discretization used. For instance, for two sub-domains each with an equidistant polar mesh with standard continuous $\mathcal{Q}_1$ finite elements, the sparsity pattern of the resulting linear system will essentially look like that shown in Fig. 2, with eight instead of four off-diagonal entries per row in $\boldsymbol{K}$. Additional information on finite element analysis for acoustic scattering can be found in [24].

5. Far-field evaluation

Once the scattered field u has been computed inside Ω, it is usually of interest to evaluate u also outside Ω during a post-processing step, either at selected locations ("receivers") or in a broader region. If integral representations that involve integration over B with the Green's function, such as (13), are used, the evaluation of u outside Ω becomes rather cumbersome and expensive. However, if the multiple-DtN approach is used, the evaluation of u at some location x in D, the region outside Ω, is inexpensive and straightforward. Indeed, since the purely outgoing wave fields u_1 and u_2 are known on B_1 and B_2, respectively, they are known everywhere outside Ω via the Fourier representation (10). In fact, we can rewrite (10) as

$$u_j(r_j,\theta_j) = \frac{1}{\pi}\sum_{n=0}^{\infty\prime} H_n^{(1)}(kr_j)\cos(n\theta_j)\frac{1}{H_n^{(1)}(kR_j)}\int_0^{2\pi} u_j(R_j,\theta')\cos(n\theta')\,\mathrm{d}\theta' + \frac{1}{\pi}\sum_{n=0}^{\infty\prime} H_n^{(1)}(kr_j)\sin(n\theta_j)\frac{1}{H_n^{(1)}(kR_j)}\int_0^{2\pi} u_j(R_j,\theta')\sin(n\theta')\,\mathrm{d}\theta', \tag{84}$$

where the two integrals correspond to the cosine and sine Fourier coefficients of $u_j|_{B_j}, j = 1, 2$. Thus, to compute $u(x) = u_1(x) + u_2(x)$ at some $x \in D$, it suffices to compute the Fourier coefficients of u_j on B_j, $j = 1,2$, yet only once. Then u_1 and u_2, and thereby $u = u_1 + u_2$, can be evaluated anywhere by summing a few terms in the Fourier representation (84) of u_1 and u_2.

Yet another quantity which is often of interest is the far-field pattern of the scattered field u. The asymptotic behavior of any solution u to the exterior Dirichlet problem (1)–(3) is

$$u(r,\theta) \sim \frac{\mathrm{e}^{\mathrm{i}kr}}{\sqrt{kr}} f(\theta), \quad r \to \infty. \tag{85}$$

The function f is called the far-field pattern of the solution. The value $f(\theta)$ is the far-field response from the scatterer in a direction θ for a given incident wave. We shall now show how to directly compute f from the values of $u_1|_{B_1}$ and $u_2|_{B_2}$. Let $c_j = (c_j^x, c_j^y)$ denote the center of B_j. The local coordinates (r_j,θ_j), relative to c_j, of a point $(r,\theta) \in D$ given in (global) polar coordinates are

$$r_j = \sqrt{(r\cos\theta - c_j^x)^2 + (r\sin\theta - c_j^y)^2}, \tag{86}$$

$$\cos\theta_j = \frac{1}{r_j}(r\cos\theta - c_j^x), \quad \sin\theta_j = \frac{1}{r_j}(r\sin\theta - c_j^y). \tag{87}$$

By combining the contributions from the various purely outgoing wave fields $u_j|_{B_j}$, $j = 1,\ldots,J$, we can then derive an explicit formula for the far-field pattern of u, given by (88) below. We summarize this result as a theorem.

Theorem 3. *The far-field pattern f defined in (85) of the solution u to the exterior Dirichlet problem (1)–(3) is entirely determined by the values of the purely outgoing wave fields u_j, $j = 1,\dots,J$, on the components B_j of the artificial boundary B, which appear in the DtN condition (56), (57). It is given by*

$$f(\theta) = \frac{1-\mathrm{i}}{\pi\sqrt{\pi}} \sum_{j=1}^{J} \mathrm{e}^{-\mathrm{i}k(c_j^x \cos\theta + c_j^y \sin\theta)} \sum_{n=0}^{\infty\prime} \frac{(-\mathrm{i})^n}{H_n^{(1)}(kR_j)} \int_0^{2\pi} u_j(R_j,\theta')\cos n(\theta-\theta')\,\mathrm{d}\theta'. \tag{88}$$

Proof. We examine the asymptotic behavior of the Fourier representation (10) of each purely outgoing wave field u_j, $j = 1,\dots,J$, for $r\to\infty$. By Taylor expansion of (86), (87) we observe that

$$r_j = r - (c_j^x\cos\theta + c_j^y \sin\theta) + \mathrm{O}(r^{-1}), \quad r\to\infty, \tag{89}$$

$$\cos\theta_j = \cos\theta + \mathrm{O}(r^{-1}), \quad r\to\infty, \tag{90}$$

$$\sin\theta_j = \sin\theta + \mathrm{O}(r^{-1}), \quad r\to\infty. \tag{91}$$

Because the angle $\theta_j \in [0,2\pi)$ is uniquely determined by the pair

$$(\cos\theta_j, \sin\theta_j) \to (\cos\theta, \sin\theta), \quad r\to\infty, \tag{92}$$

we conclude that $\theta_j \to \theta$, as $r\to\infty$, and therefore that

$$\cos n(\theta_j - \theta') \sim \cos n(\theta-\theta'), \quad r\to\infty, \quad \theta'\in[0,2\pi). \tag{93}$$

The asymptotic behavior of the Hankel functions [25] is given by

$$H_n^{(1)}(kr_j) \sim \sqrt{\frac{2}{k\pi r_j}} \exp\left\{\mathrm{i}\left(kr_j - \frac{1}{2}n\pi - \frac{1}{4}\pi\right)\right\} = \frac{\mathrm{e}^{\mathrm{i}kr_j}}{\sqrt{kr_j}} \frac{1-\mathrm{i}}{\sqrt{\pi}}(-\mathrm{i})^n, \quad r\to\infty. \tag{94}$$

From (89) we conclude

$$\sqrt{kr_j} \sim \sqrt{kr} \quad \text{and} \quad \mathrm{e}^{\mathrm{i}kr_j} \sim \mathrm{e}^{\mathrm{i}kr}\mathrm{e}^{-\mathrm{i}k(c_j^x\cos\theta + c_j^y\sin\theta)}, \quad r\to\infty. \tag{95}$$

Each purely outgoing wave field u_j, given by (10), therefore has the asymptotic behavior

$$u_j(r_j,\theta_j) \sim \frac{\mathrm{e}^{\mathrm{i}kr}}{\sqrt{kr}} \frac{1-\mathrm{i}}{\pi\sqrt{\pi}} \mathrm{e}^{-\mathrm{i}k(c_j^x\cos\theta + c_j^y\sin\theta)} \sum_{n=0}^{\infty\prime} \frac{(-\mathrm{i})^n}{H_n^{(1)}(kR_j)} \int_0^{2\pi} u_j(R_j,\theta')\cos n(\theta-\theta')\,\mathrm{d}\theta', \quad r\to\infty. \tag{96}$$

Since $u = \sum_{j=1}^{J} u_j$, the result follows by summing over j. $\square$

6. Numerical examples

We shall now combine the multiple-DtN (66), (67) and -MDtN (68), (69) condition with a finite difference scheme. We shall also compare the scattered fields obtained either with the double-DtN approach or with the single-DtN approach in a very large computational domain and demonstrate their high accuracy and convergence properties via numerical examples.

We consider the following two scatterer model problem with two obstacles, where the computational domain $\Omega = \Omega_1 \cup \Omega_2$, the obstacle boundary $\Gamma = \Gamma_1 \cup \Gamma_2$, and the artificial boundary $B = B_1 \cup B_2$:

$$\Delta u + k^2 u = f \quad \text{in } \Omega, \tag{97}$$

$$u = g \quad \text{on } \Gamma, \tag{98}$$

$$\partial_n u = \boldsymbol{T} u_{\text{out}} \quad \text{on } B, \tag{99}$$

$$\boldsymbol{P} u_{\text{out}} = u \quad \text{on } B. \tag{100}$$

To precisely describe the typical structure of the resulting discrete linear system, we consider a polar equidistant grid along B_1 and B_2. Inside Ω_1 and Ω_2, we discretize the solution with step size h_r in the r-direction and h_θ in the θ-direction. Then we use second order centered finite differences in r- and θ-direction to discretize (97). The vectors $u_N^{(1)}$ and $u_N^{(2)}$ denote the values of the numerical solution on the artificial boundary. The discretization of (97) involves the values $u_{N+1}^{(1)}$ and $u_{N+1}^{(2)}$ at "ghost" points, which lie outside the computational domain Ω. These unknown values are eliminated by using a second order finite difference discretization of (99), (100). Next, we let the vectors u_1 and u_2 denote the values of the purely outgoing wave fields on their respective boundary components. Then the discretization of the multiple-DtN condition (99), (100) is given by

$$\begin{pmatrix} \frac{2}{h_r^2}\boldsymbol{I} & \boldsymbol{0} & \boldsymbol{Q}^{(1)} & \boldsymbol{0} & \boldsymbol{M}^{(1)} & \boldsymbol{T}^{(1)}_{(2)} \\ \boldsymbol{0} & \frac{2}{h_r^2}\boldsymbol{I} & \boldsymbol{0} & \boldsymbol{Q}^{(2)} & \boldsymbol{T}^{(2)}_{(1)} & \boldsymbol{M}^{(2)} \\ \boldsymbol{0} & \boldsymbol{0} & -\boldsymbol{I} & \boldsymbol{0} & \boldsymbol{I} & \boldsymbol{P}^{(1)}_{(2)} \\ \boldsymbol{0} & \boldsymbol{0} & \boldsymbol{0} & -\boldsymbol{I} & \boldsymbol{P}^{(2)}_{(1)} & \boldsymbol{I} \end{pmatrix} \begin{pmatrix} u_{N-1}^{(1)} \\ u_{N-1}^{(2)} \\ u_N^{(1)} \\ u_N^{(2)} \\ u_1 \\ u_2 \end{pmatrix} = \begin{pmatrix} 0 \\ 0 \\ 0 \\ 0 \end{pmatrix}, \tag{101}$$

with identity matrices $\boldsymbol{I}$, all-zero matrices $\boldsymbol{0}$ and tridiagonal matrices $\boldsymbol{Q}$. The matrices $\boldsymbol{M}$, $\boldsymbol{T}$ and $\boldsymbol{P}$ are full matrices obtained by discretizing the integral operators with the second order trapezoidal quadrature rule.

A typical sparsity pattern of the entire finite difference matrix, including the discretization of (97) in the interior is shown in Fig. 2, for the special case of two circular obstacles with an equidistant polar mesh throughout Ω_1 and Ω_2. Here the ordering of the interior and boundary nodes is chosen by starting from the innermost "layers" in both domains and moving outward with increasing index. The 6 small full blocks in the lower right corner correspond to the full block-matrices in (101). In all computations below, we have used the sparse direct solver provided by Matlab. Further details about the efficient iterative solution of the system of linear equations corresponding to a *single-scattering DtN problem* can be found in [26].

6.1. Accuracy and convergence study

To demonstrate the accuracy and convergence of our method, we consider the following test problem: We let an incident plane wave impinge on a circular disk shaped obstacle centered at $(0, -d)$, with radius 0.5

Table 1
The maximal relative errors for plane wave scattering from a single obstacle, with the values of the exact solution prescribed on the boundary of the second "obstacle"

α	5×60	10×120	20×240	40×480
Relative error in the solution				
0	7.53×10^{-2}	1.77×10^{-2}	4.38×10^{-3}	1.09×10^{-3}
$\pi/4$	7.85×10^{-2}	1.84×10^{-2}	4.54×10^{-3}	1.13×10^{-3}
$\pi/2$	9.77×10^{-2}	2.24×10^{-2}	5.49×10^{-3}	1.37×10^{-3}
Relative error in the far-field pattern				
0	4.68×10^{-2}	1.11×10^{-2}	2.76×10^{-3}	6.87×10^{-4}
$\pi/4$	6.05×10^{-2}	1.45×10^{-2}	3.60×10^{-3}	8.97×10^{-4}
$\pi/2$	7.69×10^{-2}	1.85×10^{-2}	4.57×10^{-3}	1.14×10^{-3}

Incidence angle α, wave number $k = 2\pi$, DtN expansion truncated at $N = 50$, comparison with exact solution. Grids with $N_r \times N_\theta$ cells in r- and θ-direction, respectively.

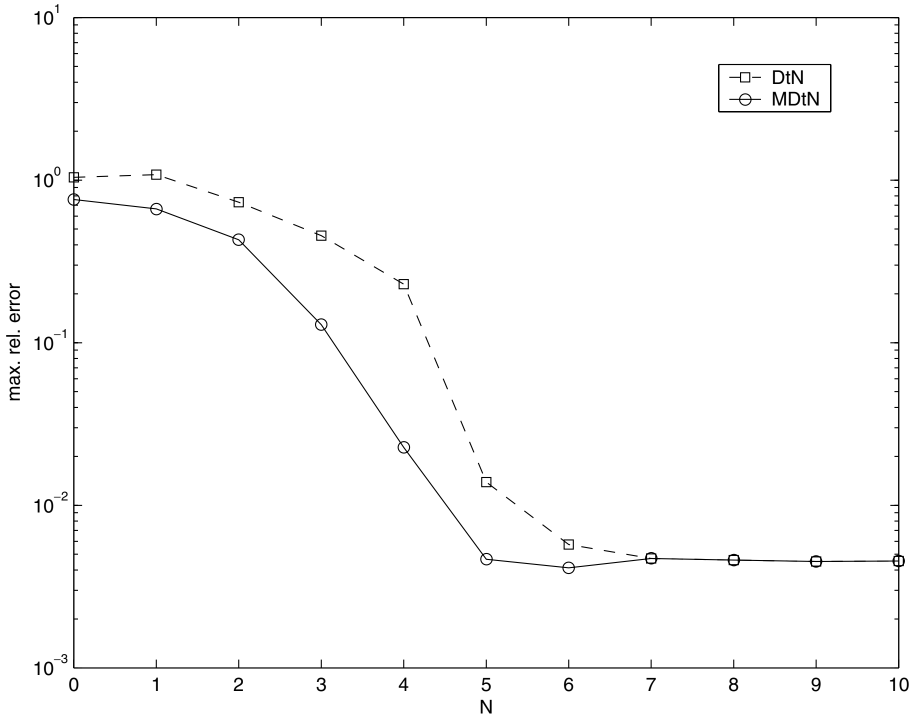

Fig. 3. The maximal relative error in the solution vs. the truncation index N, for $k = 2\pi$ and incidence angle $\alpha = \pi/4$, on the 20×240 grid. Comparison of DtN (squares) and MDtN (circles).

and distance $d = 1.5$ from the origin – see Fig. 1 for an illustration. The obstacle is located inside Ω_1 and is bounded by Γ_1. In Ω_2, no physical obstacle is present. The sound-soft boundary condition requires that the total field be zero on Γ_1, while the Jacobi-Anger expansion (see for example [19, p. 67]) yields the exact

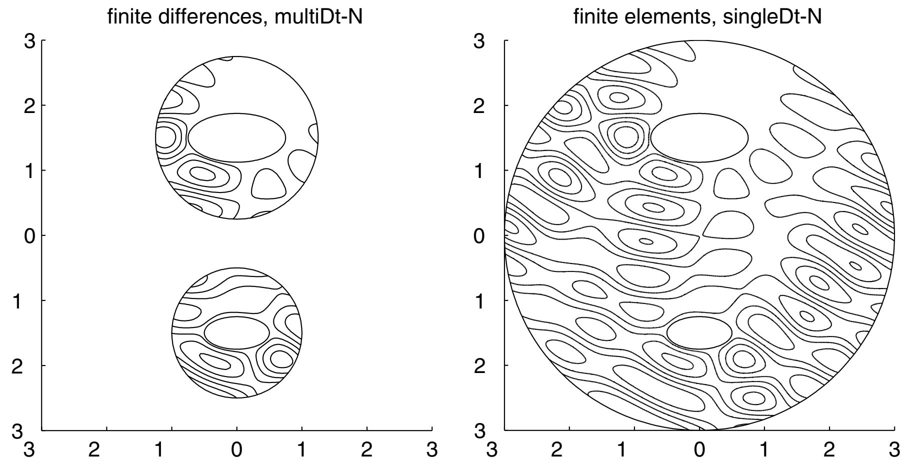

Fig. 4. Scattering from two ellipses, $k = 2\pi$, $\alpha = 3\pi/8$. Contour lines of the real parts of the total wave fields for two solutions are shown. Left: the numerical solution obtained by a second-order finite difference method combined with the multiple-DtN condition; Right: the numerical solution obtained by a (piecewise linear) finite element method combined with the single-DtN condition.

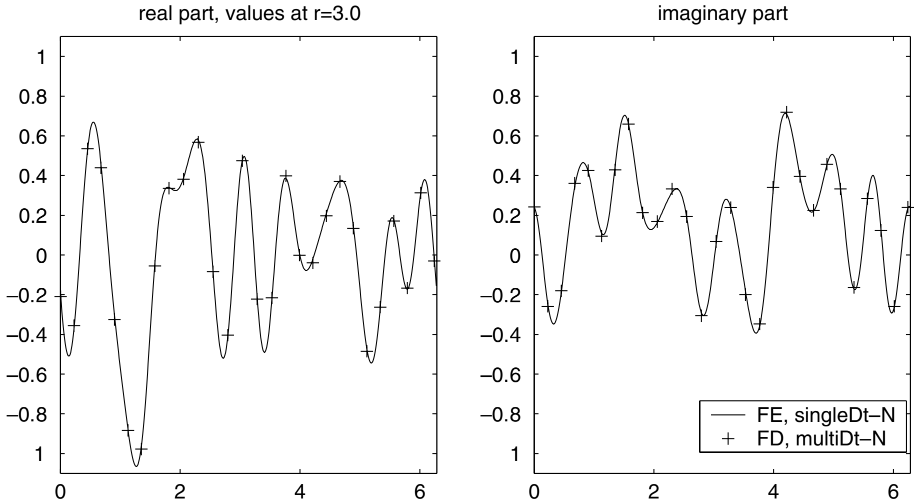

Fig. 5. Comparison of multiple-DtN with single-DtN. Values of the scattered field on the artificial boundary $r = 3$ used for the finite element solution shown in Fig. 4.

solution for the scattered field everywhere outside Γ_1. Then we prescribe its values on the boundary of a second virtual obstacle, centered at $(0, d)$ with radius 0.75, and compute the numerical solution in the two (disjoint) computational domains Ω_1,Ω_2, bounded by circles B_1 and B_2 with radii $R_1 = 1$ and $R_2 = 1.25$, respectively. We then compare the numerical result with the exact solution for single scattering.

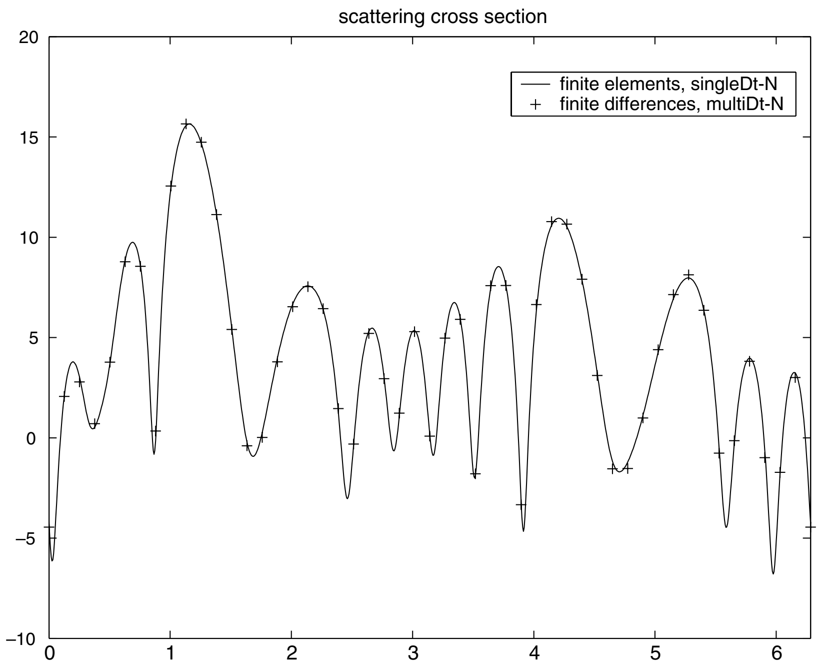

Fig. 6. Comparison of multiple-DtN with single-DtN. Values of the scattering cross-section (102) for both numerical solutions.

We choose $k = 2\pi$ for the wave number and truncate the DtN expansion at $N = 50$. We also compute the exact far-field pattern and compare it with that given by our numerical result. The maximal relative errors for different grids and incidence angles are shown in Table 1.

We observe second order convergence of our method in every case, as expected, as the mesh size $h \to 0$.

To study the effect of the truncation parameter N on the error we choose $\alpha = \pi/4$ for the incidence angle and compute the solution with varying N, either with the DtN and MDtN condition imposed at B. The relative error is shown in Fig. 3.

We observe that the modified DtN condition leads to better accuracy, even for small truncation indices N. When $N \geqslant \max\{kR_1, kR_2\}$, the two solutions computed with DtN and MDtN essentially coincide for this model problem. This behavior of the DtN and MDtN conditions illustrated in Fig. 3 is typical, and has been reported previously for single scattering problems [21,8].

6.2. Comparison with the single-DtN FE approach

Here, we consider the scattering of a plane wave with incidence angle $\alpha = 3\pi/8$ on two obstacles with sound-soft elliptic boundaries. The semi-major axes of the ellipses were chosen 0.75 and 0.5, whereas the semi-minor axes are 0.375 and 0.25, respectively. The numerical solution obtained by using our finite difference scheme with the multiple-DtN condition on the artificial boundaries is compared with a numerical solution obtained by using a finite element scheme in a larger domain, which contains both obstacles, with

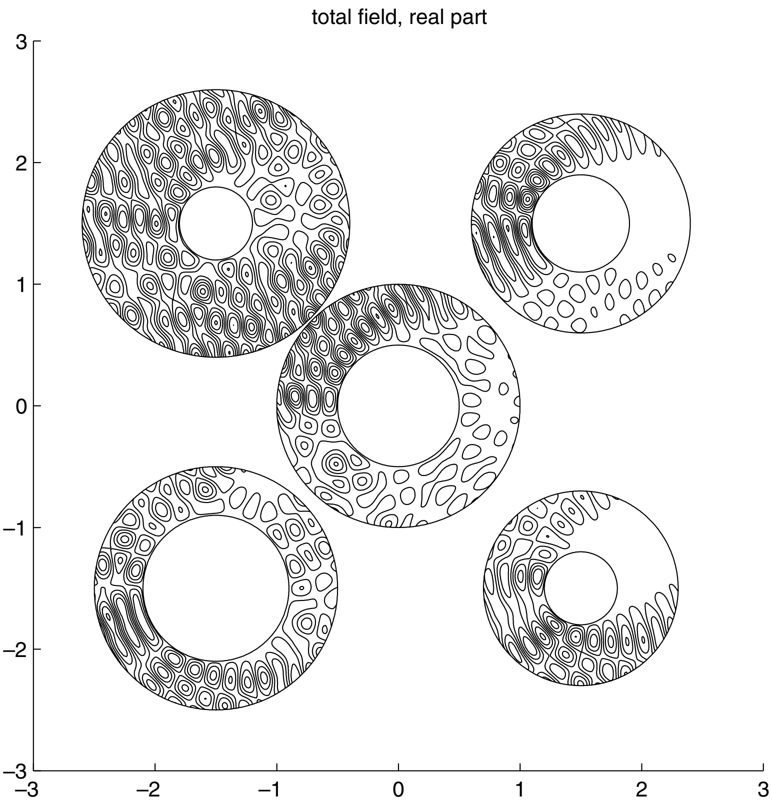

Fig. 7. The total field for plane wave scattering from five cylinders, $k = 8\pi$, incidence angle $\alpha = \pi/8$.

the single-DtN condition imposed at the artificial boundary $r = 3$. The wave number is $k = 2\pi$ and the resolutions are comparable, with about 45 grid points per wavelength. Here the modified DtN map is used and the truncation index is set to $N = 50$. The contour lines of the real part of the total field are shown for both solutions in Fig. 4. Note that the size of the computational sub-domains in the multiple-DtN case is independent of the relative distance between them, leading to a much smaller computational domain, in comparison with the single-DtN case.

In Fig. 5, the values of the two solutions on the artificial boundary at $r = 3$, which was used for the finite element solution, are shown. The multiple-DtN solution is evaluated on that boundary by using the Fourier representation (84) for the purely outgoing wave fields.

For a given far-field pattern f, the scattering cross-section $\hat{\sigma}$ is defined as

$$\hat{\sigma}(\theta) = 20\log_{10}|f(\theta)|, \quad \theta \in [0, 2\pi). \tag{102}$$

In Fig. 6, the scattering cross-section for plane wave scattering from two ellipses, obtained by using (88), is displayed for the single-DtN and multiple-DtN solutions. The two cross-sections coincide.

6.3. An example with five obstacles

An important advantage of our multiple-DtN approach is that no further analytical derivation is needed to extend it to higher numbers of scatterers, once the DtN condition is known for two domains. Here we consider the scattering of a plane wave with incidence angle $\alpha = \pi/8$ impinging on five cylindrical obstacles of different sizes with sound-soft boundaries. The wave number is set to $k = 8\pi$ and the grid consists of

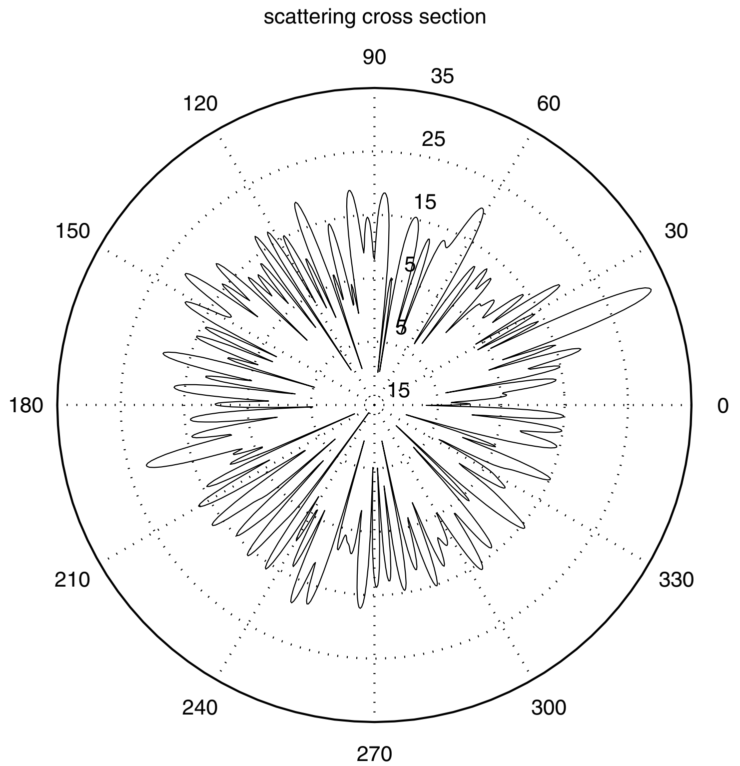

Fig. 8. The scattering cross-section (102), obtained by using (88), for the five cylinders, $k = 8\pi$, incidence angle $\alpha = \pi/8$.

about 20 points per wavelength. We use the modified DtN map and truncate the infinite series at $N = 50$. The real part of the total field and the scattering cross-section (102) are shown in Figs. 7 and 8.

7. Conclusion

We have derived a Dirichlet-to-Neumann (DtN) map for multiple scattering problems, which is based on a decomposition of the scattered field into several purely outgoing wave fields. We have proved that the corresponding DtN boundary condition is exact. When the multiple-DtN boundary condition is used to solve multiple scattering problems, the size of the computational domain is much smaller, in comparison to the use of one single large artificial boundary. In particular, the size of the computational sub-domains in the multiple-DtN case does not depend on the relative distances between the components of the scatterer. Although the artificial boundaries must be of simple geometric shape, here a circle, the DtN condition is not tied to any coordinate system inside the computational domain; in particular, it remains exact independently of the discretization used inside Ω.

We have presented a variational formulation of a multiple scattering problem with this boundary condition and also derived a formula for the far-field of the solution, which is obtained by exploiting auxiliary values used in the formulation. Accuracy and convergence have been demonstrated on a simple test problem, and a comparison with single-DtN has been made in the situation of two elliptical obstacles.

This approach is based on the decomposition of the scattered field into several purely outgoing wave fields. It can also be used to derive exact non-reflecting boundary conditions for multiple scattering problems for other equations and geometries, such as ellipses, spheres, or even wave guides, both in two and in three space dimensions, for which the DtN map with a single artificial boundary is explicitly known.

For large-scale applications in multiple scattering, it may be useful, or even necessary, to solve the sequence of sub-problems in Ω_1, Ω_2, etc. iteratively, while exchanging boundary values between the disjoint exterior boundary components via the operators M, P, and T. Parallelism can be increased even further by using standard domain decomposition techniques [27,28] separately within each sub-domain Ω_j. Although the convergence of such a Jacobi or Gauss–Seidel like iterative procedure remains an open question, it could certainly be used as an efficient preconditioner.

In this work we have only treated the time-harmonic case. In the time-dependent case, a similar approach can be used to derive exact non-reflecting boundary conditions for multiple scattering problems, by using a representation formula derived in [29]. The authors are currently investigating the time-dependent case and will report on their results elsewhere in the near future.

Acknowledgements

The authors thank Joseph B. Keller for useful comments and suggestions. They also thank Patrick Meury for his finite element code with a single-DtN boundary condition.

References

[1] B. Engquist, A. Majda, Absorbing boundary conditions for the numerical simulation of waves, Math. Comp. 31 (139) (1977) 629–651.
[2] A. Bayliss, M. Gunzburger, E. Turkel, Boundary conditions for the numerical solution of elliptic equations in exterior regions, SIAM J. Appl. Math. 42 (2) (1982) 430–451.
[3] J.-P. Bérenger, A perfectly matched layer for the absorption of electromagnetic waves, J. Comput. Phys. 114 (2) (1994) 185–200.
[4] E. Turkel, A. Yefet, Absorbing PML boundary layers for wave-like equations, Appl. Numer. Math. 27 (4) (1998) 533–557.

[5] I. Harari, M. Slavutin, E. Turkel, Analytical and numerical studies of a finite element PML for the Helmholtz equation, J. Comput. Acoust. 8 (1) (2000) 121–137.
[6] J.B. Keller, D. Givoli, Exact non-reflecting boundary conditions, J. Comput. Phys. 82 (1) (1989) 172–192.
[7] D. Givoli, Numerical Methods for Problems in Infinite Domains, Elsevier, Amsterdam, 1992.
[8] M.J. Grote, J.B. Keller, On nonreflecting boundary conditions, J. Comput. Phys. 122 (2) (1995) 231–243.
[9] D. Givoli, Recent advances in the DtN FE method, Arch. Comput. Methods Engrg. 6 (2) (1999) 71–116.
[10] G.K. Gächter, M.J. Grote, Dirichlet-to-Neumann map for three-dimensional elastic waves, Wave Motion 37 (3) (2003) 293–311.
[11] P.A. Martin, Multiple Scattering, an Invitation, in: G. Cohen, et al. (Eds.), Proceedings of the 3rd International Conference on Mathematical and Numerical Aspects of Wave Propagation, SIAM, Philadelphia, 1995, pp. 3–16.
[12] P.A. Martin, Integral-equation methods for multiple-scattering problems. I. Acoustics, Quart. J. Mech. Appl. Math. 38 (1985) 105–118.
[13] P.A. Martin, F.J. Rizzo, Partitioning, boundary integral equations, and exact Green's functions, Int. J. Numer. Methods Engrg. 38 (1995) 3483–3495.
[14] F. Záviška, Über die Beugung elektromagnetischer Wellen an parallelen, unendlich langen Kreiszylindern, Ann. Phys., Folge 4 (40) (1913) 1023–1056.
[15] B. Peterson, S. Ström, Matrix formulation of acoustic scattering from an arbitrary number of scatterers, J. Acoust. Soc. Amer. 56 (3) (1974) 771–780.
[16] V. Twersky, On multiple scattering of waves, J. Res. Nat. Bur. Standards 64D (1960) 715–730.
[17] J.E. Burke, V. Twersky, On scattering of waves by many bodies, J. Res. Nat. Bur. Standards 68D (1964) 500–510.
[18] F.M. Arscott, A. Darai, Curvilinear coordinate systems in which the Helmholtz equation separates, IMA J. Appl. Math. 27 (1981) 33–70.
[19] D. Colton, R. Kress, Inverse Acoustic and Electromagnetic Scattering Theory, Springer, 1992.
[20] D. Colton, R. Kress, Integral Equation Methods in Scattering Theory, Wiley-Interscience, 1983.
[21] I. Harari, T.J.R. Hughes, Analysis of continuous formulations underlying the computation of time-harmonic acoustics in exterior domains, Comp. Methods Appl. Mech. Engrg. 97 (1) (1992) 103–124.
[22] J.-C. Nédélec, Acoustic and Electromagnetic Equations, Integral Representations for Harmonic Problems, Springer, 2001.
[23] I. Harari, I. Patlashenko, D. Givoli, Dirichlet-to-Neumann maps for unbounded wave guides, J. Comput. Phys. 143 (1) (1998) 200–223.
[24] F. Ihlenburg, Finite Element Analysis of Acoustic Scattering, Springer, 1998.
[25] M. Abramowitz, I.A. Stegun, Handbook of Mathematical Functions, Dover Publications, 1970.
[26] A.A. Oberai, M. Malhotra, P.M. Pinsky, On the implementation of the Dirichlet-to-Neumann radiation condition for iterative solution of the Helmholtz equation, Appl. Numer. Math. 27 (4) (1998) 443–464.
[27] J.-D. Benamou, B. Després, A domain decomposition method for the Helmholtz equation and related optimal control problems, J. Comput. Phys. 136 (1) (1997) 68–82.
[28] M. Balabane, A domain decomposition algorithm for the Helmholtz equation. 1 – The dissipating case. Asymptot. Anal., in press. Also available as preprint at: http://www-math.math.univ-paris13.fr/prepub/pp2003/pp2003-01.html.
[29] M.J. Grote, C. Kirsch, Far-field evaluation via nonreflecting boundary conditions, in: Th.Y. Hou, E. Tadmor (Eds.), Proceedings of the 9th International Conference on Hyperbolic Problems (Hyp2002), Springer, 2003, pp. 195–204.